

## Role of fracture toughness in impact-abrasion wear

A.R. Chinth<sup>a,b,\*</sup>, K. Valtonen<sup>c</sup>, V.-T. Kuokkala<sup>c</sup>, S. Kundu<sup>b</sup>, M.J. Peet<sup>a</sup>, H.K.D.H. Bhadeshia<sup>a</sup>

<sup>a</sup> University of Cambridge, UK

<sup>b</sup> Tata Steel Ltd., India

<sup>c</sup> Tampere University, Finland

### ARTICLE INFO

#### Keywords:

Wear testing  
Steel  
Abrasion  
Impact-abrasion  
Fracture toughness

### ABSTRACT

Two new low alloyed steels were developed with different fracture toughness values but at similar level of hardness with same composition and microstructural phase. The steels were subjected to impact-abrasion wear test. This work examines specifically the additional role of toughness during impact-abrasion wear, using a newly developed high toughness steel. Microstructural characterisation of the damaged samples revealed that better toughness helps resist both impact and abrasion damage.

### 1. Introduction

Impact-abrasion includes the effects of both the collision of abrasive particles with the solid surface, and scratching motions; other factors such as particle size, shape, environment and rate of impact and abrasion, together make this a complex problem [1,2]. The phenomenon itself is of considerable importance in the wear-resistant steels used in earth-moving equipment such as excavators and loaders, and machines used in mining operation. Abrasion per se correlates strongly with hardness, although it is well-established that hardness alone does not always explain the wear behaviour [3–11]. For instance, abrasion wear resistance of commercially available steels showed no correlation with their hardness [4]. Loss of material in a phenomenon such as impact abrasion is likely to have some dependence on the failure mechanism [12].

For instance, during abrasive wear, removal of material from the surface occurs when the strain there reaches a critical value. This local fracture-strain may be achieved by a single or multiple abrasive strikes at the surface. Material not removed in this way may nevertheless deform as a result of the abrasion and impact event [13]. It therefore is reasonable to expect that steels with a large fracture stress and work hardening rate should have high wear resistance. For example, it is established that in the rails, the work hardening capacity plays a key role in determining the wear rate of pearlitic steels which perform better than harder martensitic alloys [7]. Hadfield steel is good at resisting wear due to its high work hardening capacity, but when used for ore crushing, it suffers severely from impact-abrasive wear [14]. This is because wear of this kind can be dominated by microscopic cracking resulting from the combination of plasticity and impact, emphasizing

the need to consider toughness as a parameter in controlling material removal. This is obvious in brittle materials such as ceramics [15–18].

The purpose of the work presented here was to examine specifically the role of toughness of a newly developed steel on impact abrasion.

### 2. Material and experimental details

A new low alloyed steel (Table 1) with a unique combination of properties in the hot-rolled condition, has been designed, mass produced, and tested. Usually, for a given strengthening mechanism, increase in strength comes at the cost of reduced toughness. Increasing toughness and strength in combination is therefore non-trivial and requires the introduction of specific additional toughening mechanisms. Refinement of the microstructure is the one general mechanism which is known to improve both strength and toughness. Microalloying with vanadium was identified a method for achieving refinement of the austenite grain size during processing (and therefore to reduce the maximum size of the martensite plates) [19]. Ni at low amount of Mn was added to increase toughness, and Cr and Mo were added to increase hardenability [20,21]. Si was added to avoid formation of carbide formation during cooling [22].

The steel has a hardness of  $561 \pm 23$  HV and a tensile strength of  $2.0 \pm 0.01$  GPa, still maintaining a fracture toughness of  $72 \pm 1.5$  MPa $\sqrt{m}$ . The steel was thermomechanically processed to obtain severely pancaked austenite and then naturally cooled in ambient conditions to room temperature to generate a martensitic microstructure. The steel has high hardenability and hence it can transform into martensite at cooling rates as low as  $1 \text{ K s}^{-1}$ . The final thickness of the hot-rolled plates was 6 mm.

\* Corresponding author. University of Cambridge, Materials Science and Metallurgy, 27 Charles Babbage Road, University of Cambridge, Cambridge CB3 0FS, UK.  
E-mail addresses: [ac2044@cam.ac.uk](mailto:ac2044@cam.ac.uk), [apparao@tatasteel.com](mailto:apparao@tatasteel.com) (A.R. Chinth).

**Table 1**  
Composition of the steel in wt%.

C	Si	Cr	Ni	Mo	V	Al	S	P
0.34	1.45	1.5	3.53	0.39	0.3	0.01	0.005	0.005

There are a number of applications envisaged for the alloy, but of particular interest is its use in conditions where it would sustain damage from a combination of impact and abrasion. For this reason, some of the steel was heat treated such that its hardness was maintained, but the toughness was not. To do this, the steel was re-austenitised to destroy the hot-rolled microstructure followed by quenching to room temperature, in which case the hardness was measured to be  $666 \pm 23$  HV. The steel was also tempered at  $190^\circ\text{C}$  for 2 h to reduce the hardness to  $585 \pm 5$  HV in order to match that of the as-rolled steel. The hot-rolled steel was also tempered for 2 h to additionally study its wear resistance in the tempered condition. Wear results of all the four variants (hot-rolled, hot-rolled and tempered, quenched, and quench and tempered) are discussed, but the detailed characterisation is limited to the hot rolled and quenched steels. Nevertheless, the additional variants enhance the comparison of the wear rate and its dependence on hardness, as will be seen later on.

Impact-abrasion tests were carried out using an impeller-tumbler testing machine available at Tampere University, Finland. Details of the machine have been discussed elsewhere [23]. Known alternatively as a continuous impact-abrasion test [24], it has been used to test wear resistant steels destined for the mining industry [24–26]. The associated conditions are not as severe as in grinding and crushing, but are greater than those generated in the dry sand rubber wheel test. The machine consists of an impeller shaft carrying samples in a rotating drum containing abrasives. Multiple samples can be mounted at different angles relative to the sample holder tangent. The abrasive can be ore, or typically granite particles in the size range of 8–20 mm [27,28]. The size range is consistent with the simulation of wear in mining equipment [29]. The amount of abrasive can be varied, but it is usually in the range of 400–900 g [25,28].

The entire assembly is enclosed within the drum and the impeller shaft allowed to rotate in the same sense. The test sample has the dimensions  $75 \times 25$  mm. The shaft with samples attached is rotated at  $700 \pm 5$  rpm, while the drum is rotated in the same direction at 30 rpm. There is a simultaneous application of impact from different angles and abrasion from sliding of the particles against the sample surface. The abrasive fractures during the test so that the conditions can change with time. To avoid this, the abrasives are changed after every 15 min of testing. The procedure is repeated for a total testing time of 1 h or more, with the weight loss measured at hourly intervals. Three readings were obtained for each measurement, and the test was repeated with two different samples for each condition.

The test parameters implemented in the present study are listed in Table 2, chosen to be similar to those in the published literature [30]. The Kuru granite used in this work has the same crushability, about 38% [31], but relatively lower abrasiveness (1380), while Sorila granite used in the reference work had 1500. In both granites, the abrasiveness

**Table 2**  
Impeller-tumbler test parameters.

Sample dimensions	75 mm $\times$ 25 mm $\times$ 6 mm
Rotation speed impeller	700 $\text{min}^{-1}$
Rotation speed tumbler	30 $\text{min}^{-1}$
Abrasive size	10–12.5 mm
Abrasive mass	900 g
Test duration	240 min
Abrasive	Granite (Kuru quarry, Finland)
Sample angle	$60^\circ$

is clearly in an extreme abrasive range [25]. Although there is a small difference in the abrasiveness measured with the LCPC (Laboratoires des Ponts et Chaussées, Paris) method [31], the results from this work can be compared with the reference data. Kuru granite was originally crushed with a jaw crusher in the quarry and then sieved to the selected 10–12.5 mm particle size.

Samples for scanning electron microscopy (SEM) were polished electrolytically in 80% methanol, 15% glycerol and 5% perchloric acid, at  $5\text{--}10^\circ\text{C}$ , 10 V for 2–5 min depending on the sample dimension.

Surface roughness of the tested samples was measured as an arithmetic average ( $R_a$ ) of the profile height deviations from the mean. It was measured using a single scan surface profilometer, DEKTA 6M. A load of 10 mg was applied. Six profile readings were obtained for each tested condition. The length of each profile was 10 mm with a scan time of 120 s.

SEM was carried out using FEI Nova NanoSEM, fitted with Everhart-Thornley and through-the-lens secondary electron detectors, and in-lens type backscattered electron detector for microstructural characterisation, operated at 10–15 kV and a working distance of 4–13 mm. Phenom Pro X desktop SEM fitted with silicon drift detector was used to obtain elemental information of granite. Electron backscattered diffraction data was obtained by using FEI Quanta 3D FEG-SEM with a step size of  $0.4\text{--}0.5\ \mu\text{m}$  and the data was analysed using Oxford Instruments AZtecHKL.

### 3. Results and discussion

Fig. 1 shows the hot-rolled structure exhibiting severely pancaked unrecrystallized austenite grains, which contain deformation bands. These defects ensure a fine martensite structure which is conducive to good toughness since the tendency to crack under load decreases with plate size [32]. Further, it is proven experimentally that a decrease in

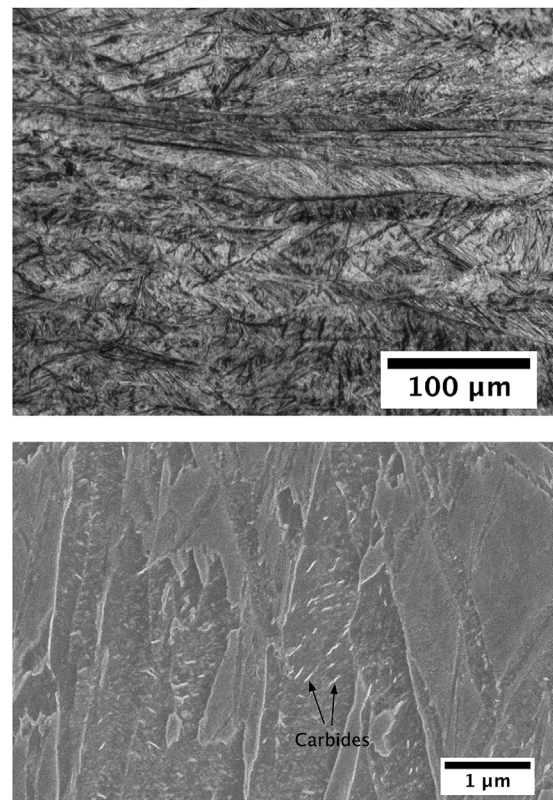


**Fig. 1.** (a) Hot-rolled steel showing pancaked prior-austenite grains, which transform into fine martensite during cooling. (b) Higher resolution image showing that the structure contains some autotempered martensite.

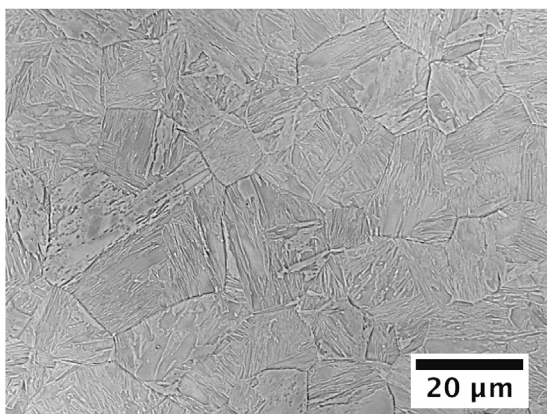


Fig. 2. Martensitic microstructure of the re-austenitised and quenched steel, showing coarse and equiaxed prior austenite grains.

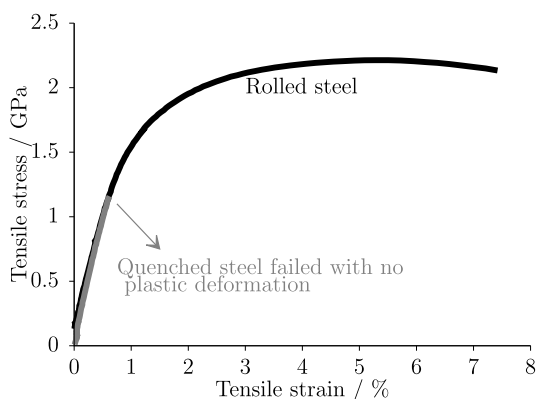


Fig. 3. Engineering stress - strain curves of the rolled steel, and of the re-austenitised and quenched steel. The quenched steel fractured at about 1.16 GPa with negligible plastic deformation.

prior austenite grain size reduces the packet and block size [33–35]. In this condition, the steel has a hardness of  $561 \pm 23$  HV30 and a fracture toughness of  $72.0 \pm 1.5$  MPa $\sqrt{m}$ .

To investigate the role of fracture toughness on impact-abrasion, a simple experiment was designed in which the hot-rolled steel was

re-austenitised at 900 °C for 1 h and quenched so that the scale of the microstructure increases and the toughness decreases. The resulting microstructure is shown in Fig. 2. The austenite grain size was measured with the linear intercept method and found to be  $12.3 \pm 1.5$   $\mu$ m.

The steel plate thickness of 6 mm prevents conventional fracture toughness tests. Tensile tests were therefore carried out to determine the ductility. It is evident from Fig. 3 that the quenched steel broke in a brittle manner before plastic yielding, whereas the hot-rolled steel behaved in a ductile manner. Fig. 4 shows the mixed mode tensile fracture surface of the rolled sample, consisting of ductile dimples and quasi-cleavage. In contrast, brittle cracks and cleavage facets are evident in the case of quenched samples.

The {100} pole figure of the martensite from a single parent austenite crystal for the hot-rolled, and the quenched sample is shown in Fig. 5. Each austenite grain in the hot-rolled steel is severely deformed and fragmented, gaining a large spread of misorientation in the martensite generated on cooling. In contrast, the martensite that formed in the undeformed austenite has a much smaller spread in orientations. The martensite in the hot-rolled structure expected to be much tougher, for two reasons. Firstly, the crystallographic grain size, which controls the cleavage mode of fracture [36] and secondly because fine plates of martensite have a reduced tendency to crack [32]. Therefore, from the {100} pole figures, the tensile test results and fracture surface analysis, it can be assumed that the fracture toughness in the austenitised and quenched is lower compared to the rolled steel.

In the discussion that follows, the hot-rolled steel will be referred to as “hot rolled” and the re-austenitised steel as “quenched”.

### 3.1. Wear test results

The relative wear loss data, the weight losses relative to that of a reference sample, R400 with 400 BHN, are plotted in Fig. 6 and listed in Table 3. The tests were done in conditions comparable to those of the published work [30]. Fig. 6 shows that the wear loss of the reference samples (R400, 450, 500) indeed correlate with hardness, but it is evident that our hot-rolled steel, which is softer than the re-austenitised and quenched version, has better wear performance, confirming that its better toughness prevails. Furthermore, at essentially the same hardness, the hot-rolled steel performs far better than steel R500 [25]. The relative wear loss of the rolled samples is about 17% less than that of the quenched samples. The standard deviation of the many samples tested in the impact-tumbler test evaluated to be less than 4% [30], and

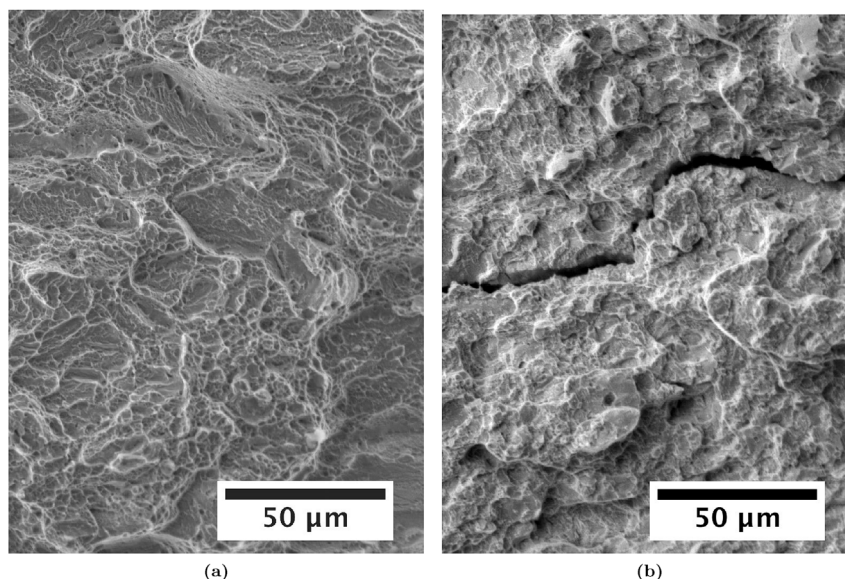


Fig. 4. (a) Micrograph of a fractured rolled steel revealing ductile and quasi-cleavage features. (b) Brittle fracture of the quenched steel.

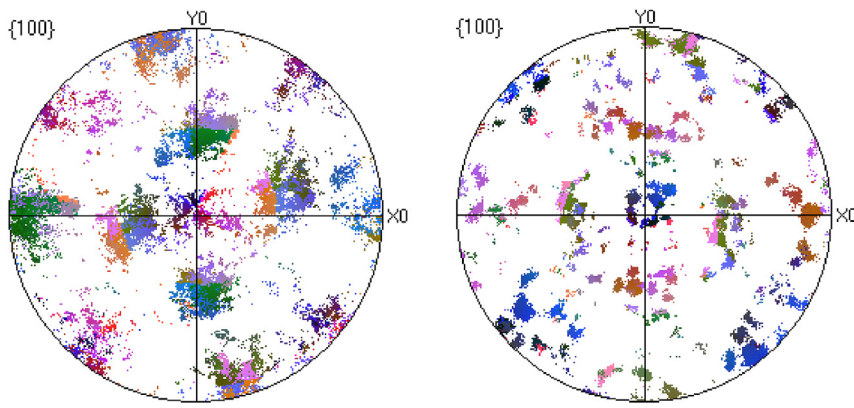


Fig. 5. {100} pole figure from a parent austenite grain of (a) hot-rolled, and (b) quenched steel. Variants spread is more in the hot-rolled steel compared to the quenched steel. The data consist of about 17 000 poles in both the steels. RGB color scheme denotes martensite variants. (For interpretation of the references to color in this figure legend, the reader is referred to the Web version of this article.)

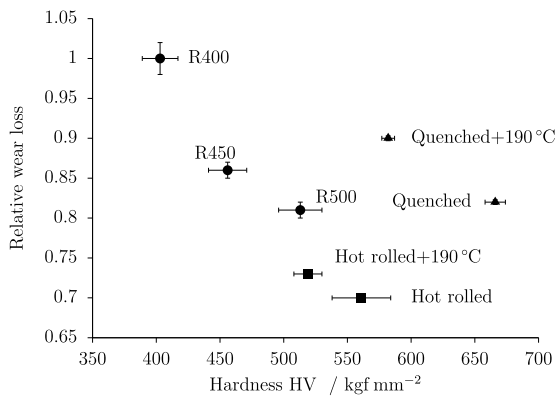


Fig. 6. Relative wear loss of different steels plotted against their hardness. The triangles represent the heat treated samples of hot-rolled steel, and the filled squares the hot-rolled steel.

Table 3  
Relative wear loss in comparable steels.

Sample	Hardness/HV30	Relative wear loss
Hot rolled	561±23	0.700±0.003
Hot rolled and tempered at 190° for 3 h	519±11	0.730±0.003
Quenched	666±8	0.820±0.003
Quenched and tempered at 190° for 3 h	582±5	0.900±0.003
R400	395±14	1.00±0.02
R450 [30]	450±15	0.920±0.010
R500 [30]	515±17	0.880±0.010

it is about 2% for the reference samples in these tests. Therefore, it is evident that the wear loss in the much harder quenched samples is at least 10% higher than that of the rolled samples.

A novelty of the present work is that it reports experiments where toughness is varied greatly, while maintaining a martensitic microstructure and hardness. The martensite in the hot-rolled sample is in a greatly refined state, reflected in its high toughness and ductility. A previous study could not be conclusive because hardness, toughness, microstructure and alloy composition were not controlled to enable clear comparisons [37].

3.1.1. Surface roughness

Surface roughness of the tested samples as well as comparative data on pearlitic and bainitic steels tested in dry sand rolling/sliding wear tests are listed in Table 4. All the impact-tumbler test results shown were generated under identical conditions. Compared to pure abrasion, impact-abrasion exacerbated roughness. Pure abrasion involves material removal through microcutting and micro-fatigue, so it is not surprising that it leads to a lower roughness. Impact-abrasion, in contrast,

Table 4  
Surface roughness after impact-abrasion testing compared to previous studies, varying steel microstructures, and test methods.

Sample	Test type	Surface roughness/μm
Hot rolled	Impeller-tumbler	5.8±0.4
Hot rolled, tempered at 190° <sub>c</sub> , 3 h	Impeller-tumbler	6.6±0.5
Quench	Impeller-tumbler	6.3±0.5
Quenched, tempered 190° <sub>c</sub> , 2 h	Impeller-tumbler	6.7±0.2
R400	Impeller-tumbler	8.2±1.0
R450	Impeller-tumbler	9.1
R500	Impeller-tumbler	8.0
S355	Impeller-tumbler	15.1
R400	Uniaxial crusher	10.1
R400	Pin on disc	8.0
R450	Uniaxial crusher	7.9
R500	Pin on disc [30]	6.0
R500	Uniaxial crusher [30]	7.0
Pearlite	Dry sand rubber wheel [38]	3.0
Bainite	Dry sand rubber wheel [38]	1.1

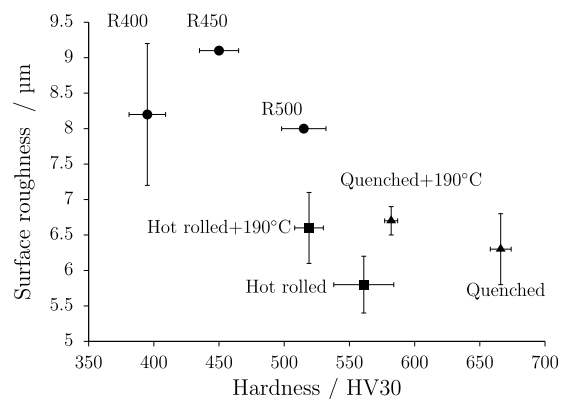
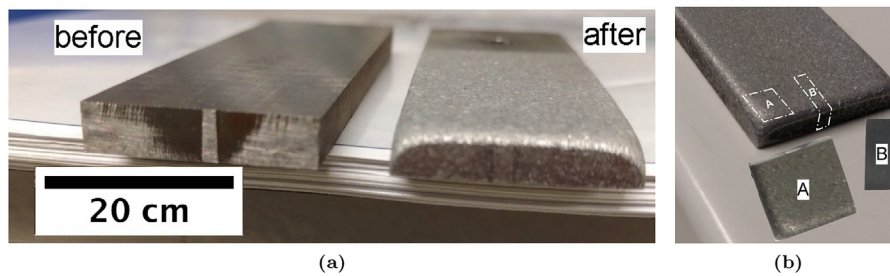


Fig. 7. Roughness of the surface of the tested samples. The data for the R450 and R500 samples are from Ref. [30].

includes chipping and fragmentation. Fig. 7 shows that the roughness does not correlate well with hardness for any of the samples. The newly developed steel shows similar roughness values, although the roughness of the rolled sample is marginally lower. To understand these observations, the worn surface was characterised using a number of techniques.

Unlike in the case of pure abrasion, the wear caused by impact-abrasion is not uniform across the sample surfaces (Fig. 8). The worn sample edge resembles the rounded tip of the cutting edges of a typical mining loader bucket [39]. Samples for the surface as well as for the



**Fig. 8.** (a) Impeller-tumbler samples before and after testing. (b) The areas marked as 'A' and 'B' were cut for the further characterisations. 'A' (10 × 10 mm) was used to characterise the surface, while 'B' (10 × 5 mm) was used for the cross sectional studies.

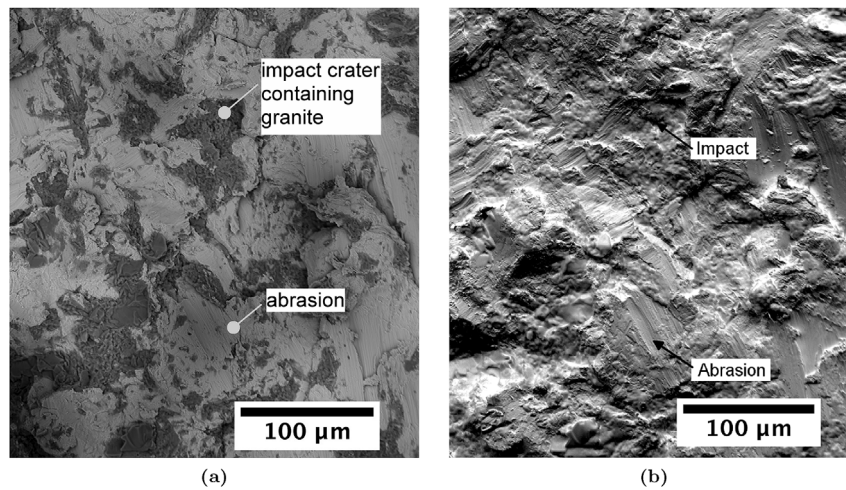


**Fig. 9.** Backscattered electron images of the worn surface of a hot rolled sample, (a) illustrating two distinctive regions of wear: impact and abrasion. (b) Topography of the same area as in (a). The flat regions in (b) show abrasion in different directions.

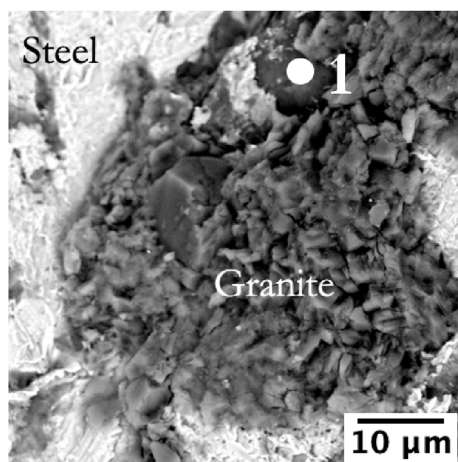


**Fig. 10.** Shows a granite particle in an impact crater. The granite essentially contains oxides of Al and Si.

cross sectional microstructural studies were cut as marked in Fig. 8b. Sample 'A' (10 × 10 mm) was used to characterise the surface, while sample 'B' (10 × 5 mm) was used to study the cross section.

A typical surface of the tested sample is shown in Fig. 9. The backscatter electron images reveal darker-contrast regions containing granite, which contains silicates and oxides with low atomic number elements, including, Si, Al, and O, as confirmed using energy dispersive X-ray spectroscopy, Fig. 10 and Table 5. The topography of the same area as in Fig. 9a can be seen in 9b. A typical impact crater and abrasion are marked in Fig. 9b. The abraded regions are relatively bright compared to the regions of impact, and uniform in their contrast due to

**Table 5**

Contents of the granite obtained by energy dispersive X-ray analysis from the region marked '1' in Fig. 10.

Element	At. conc.	Wt. conc.
O	0.50	0.33
Si	0.26	0.31
Al	0.11	0.12
Fe	0.08	0.18
Na	0.03	0.02
Ca	0.02	0.03
K	0.006	0.01

their small roughness. The rougher impact regions are darker and less resolved. It is noteworthy that the directions of the abrasion scratches are not constant, as would be expected from three-body or two-body abrasion wear. Some areas indicate delamination, which is one of the key damage mechanisms in sliding or abrasion wear [40].

The damage modes observed in impact-abrasion are shown in Fig. 11. The test consists of many chaotically moving granite particles impacting the test surface at different angles from 0 to 90° and also at varying velocities. Near 0°, the damage is abrasive, involving micro-cutting, wedge formation and microplothing. At other angles of impact, the material is displaced or removed from the site of the impact depending on the impact energy, and also impact craters are developed. When the impact occurs approximately normal to the surface, the displaced material from the crater is distributed as a lip around the crater, although some material may also be ejected from the sample, depending on the energy of the impact. An example is illustrated in Fig. 11a, where the impact was at an acute angle with material piling up on the sides of the crater. The crater itself contains some of the granite responsible for the damage. At the exit side of the impact, small

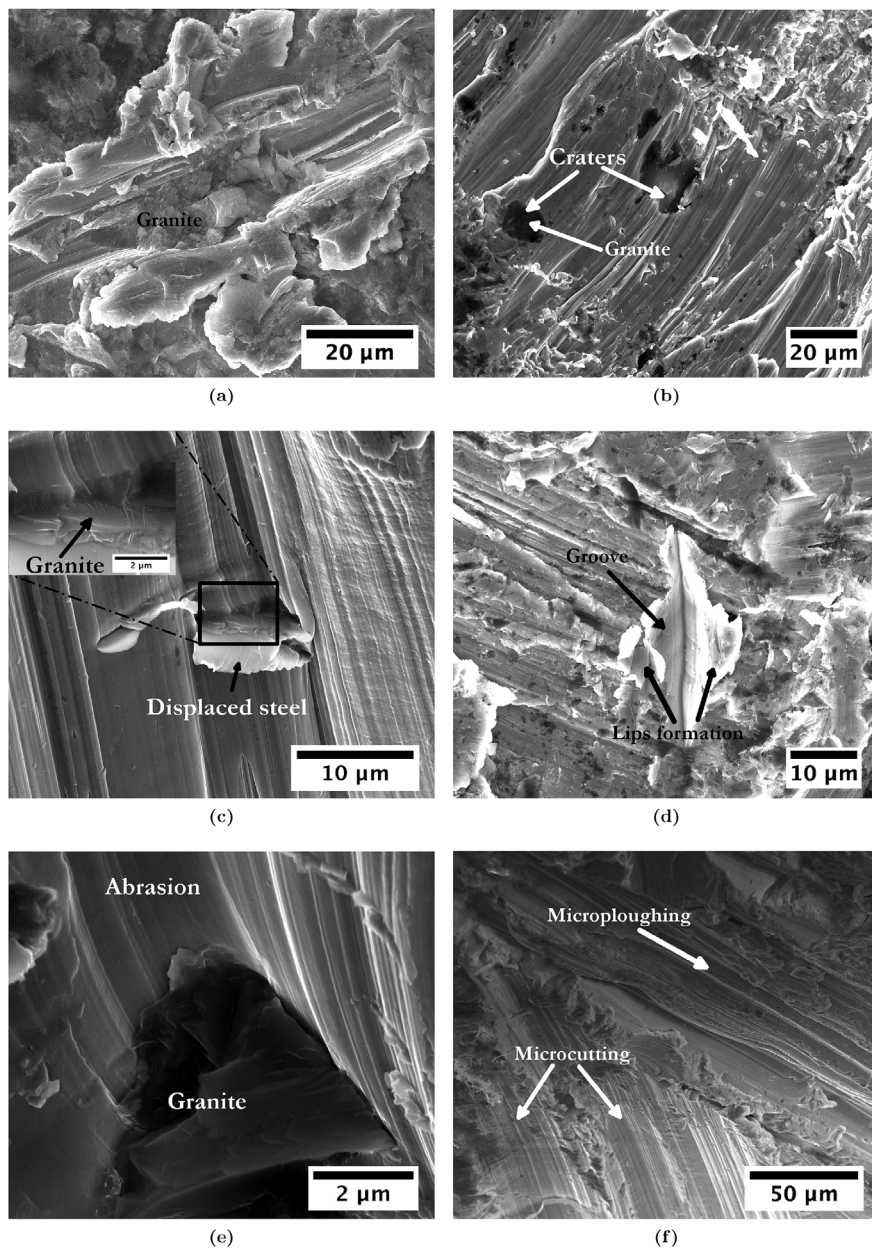


**Fig. 11.** Surface topography of the tested samples after 4 h of testing. The images illustrate the impact-abrasion wear in general, (a) and (b) showing craters formed by impacts, (c) and (d) cutting by the abrasives, and (e) and (f) abrasion due to moving granite particles. (a), (c) and (e) are from the quenched steel, while the rest of the images are from the hot-rolled steel.

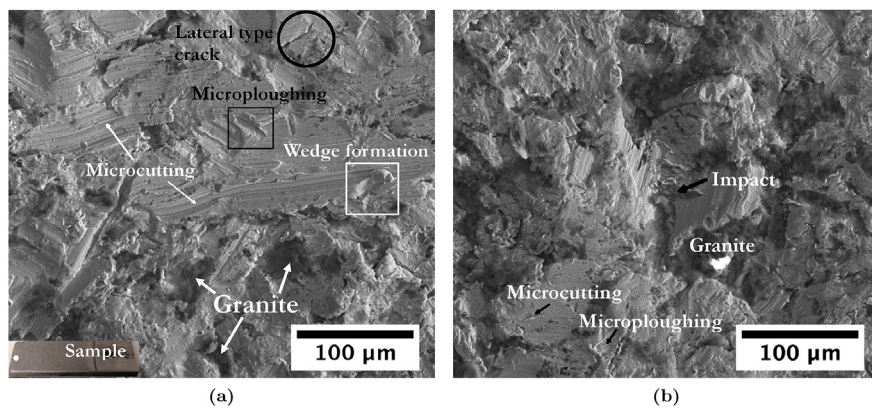


**Fig. 12.** Surface topography following 4 h of testing, (a) a hot-rolled sample, (b) quenched sample.



Fig. 13. The cross section sample 'B' shown in Fig. 13 of the impact-tumbler sample. Abrasion predominates in region '1', and impact damage in regions '3', with region '2' representing a transition area.

chips of the steel can be noticed, and hence the process of such removal can be classified as microchipping.

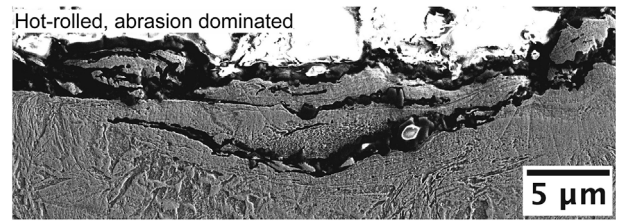
Other impact incidents where the sharp edges of granite particles has caused the formation of a groove and lips are shown in Fig. 11c and 11d. The removal of material is similar to that of micromachining reported in the previous investigations [41]. However, in the impact shown in Fig. 11d, in which there is no debris left as in the previous impact example, the lips are severely strained. Any lips that form also act as obstacles for the abrasion by granite and hence can be removed by subsequent action. Intense shear of remaining material can occur during the removal process. A case of abrasion after an impact event is shown in Fig. 11b. There are two craters, one containing granite (on the left hand side of the image), and another without any debris.

It is possible that the embedding of hard granite particles in the steel during the process of impact abrasion actually enhances its resistance to further damage, but creating in effect a metal matrix composite. It is known that in the case of quartz particles, that their embedding leads to a better pin-on-disc wear resistance when the substrate has a hardness in the range 400–800 HV, but spalling becomes easier when the substrate is soft [42]. The steels characterised in this study fall in a fairly narrow hardness range of 525–675 HV, so the mechanism of embedded particles should be identical and therefore not affect the ranking in terms of wear loss. There is a caveat to the comparison with the quartz experiments, that the present study involves both severe impact and abrasion, so there are many cracks created in the embedded granite particles, which may render them liable to detachment. However, these phenomena warrant further studies.

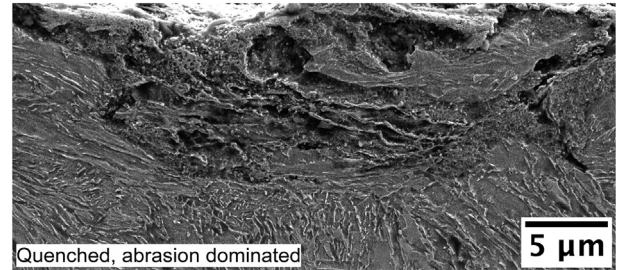
Fig. 12 shows a comparison between the hot-rolled and quenched samples. Although the same mechanisms of damage are apparent in both samples, the quenched samples show much more brittle behaviour with smaller extents of microcutting regions.

### 3.2. Microscopy of sections

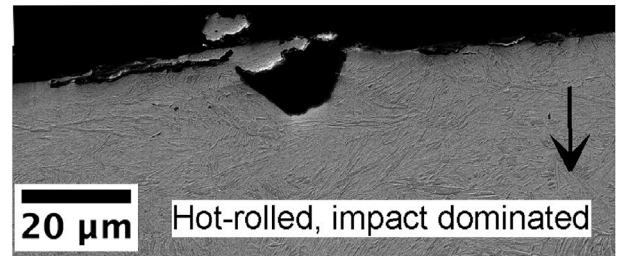
Dominant wear mechanisms in the cross section sample 'B' are shown in Fig. 13. Representative micrographs from the abrasion and impact dominant mechanisms are presented in Fig. 14. Data from about ten for the hot-rolled and about twenty for the quenched measurements are listed in Table 6. In general, the hot-rolled and quenched steels show similar abrasion resistance, although the material within the abraded regions seems to be more damaged in the latter case (Fig. 14). On the other hand, the craters in the impact zone, which represent the biggest surface of the impact-tumbler sample, are largest for the



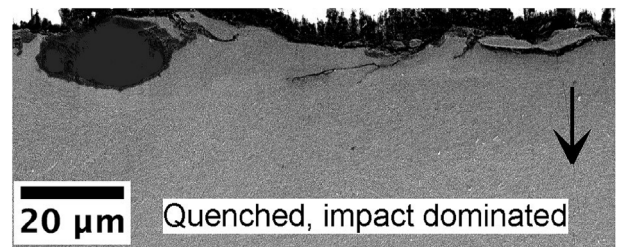
(a)



(b)



(c)



(d)

Fig. 14. Metallography of the predominantly abrasion and impact resistant regions illustrated in Fig. 13. The arrows show the direction of impact in (c) and (d).

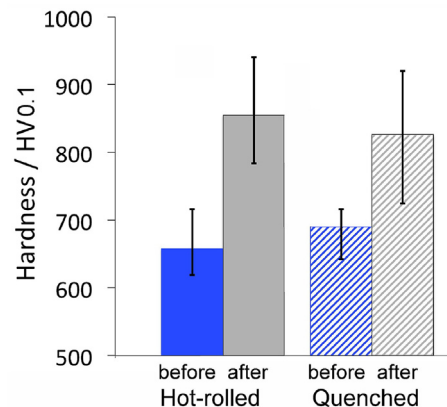


Fig. 15. Hardness data obtained using a 0.1 kgf load to assess the surface hardening after wear testing. The "error" bars in this case illustrate the maximum and minimum values recorded.

**Table 6**

Depth of the craters in due to impacts on the test surface. Abrasion-dominated and impact-dominated regions are illustrated in Fig. 13.

Sample	Abrasion dominated region	Impact dominated region
Hot-rolled steel	5.0±1.7 μm	7.5±3.7 μm
Quenched steel	6.5 ± 2.0 μm	15.8±5.5 μm

quenched steel, and there also seem to be cracks associated with the craters in the steel. This must be a consequence of the low toughness in quenched steel compared to the hot-rolled steel, which explains why the wear rate is greater for the quenched steel even though it is much harder than the hot-rolled grade.

Further, the hot-rolled steel strain hardens during wear to a greater extent than the quenched grade (Fig. 15), presumably because of its greater ductility. It is well known that surface hardening, leads to improved wear resistance in many abrasion scenarios [37,43].

#### 4. Conclusions

This study is the first of its kind to develop steels with two levels of toughness without changing either composition or microstructural phase, and at similar hardness level. We have demonstrated here that under the given circumstances, the steel with a better toughness outperforms a harder and relatively brittle steel.

In hindsight, this result may look quite obvious, but the work reveals two mechanisms that rely on toughness and ductility in addition to hardness. The first is that the abrasion wear resistance of the steel is clearly better when it is tougher, because the material that is extruded by the abrasive action is more likely to detach from a brittle steel. On the other hand, and even more interestingly, the wear resistance did not show a significant difference between the two steels, when the impact-dominated regions of the samples were studied. Secondly, the steel with the greater ductility revealed a greater hardness in the vicinity of the wear surfaces after the impact-tumbler tests. Despite the fact that the quenched grade had a greater initial hardness, the hot-rolled steel had a greater capacity to work harden given its much larger ductility.

Further investigation of the damaged surface and subsurface is required to understand the impact-abrasion damage mechanism in general and the role of toughness in changing the wear mechanism. 3D SEM and X-ray tomography may help in revealing the damage mechanism at surface and subsurface level.

#### Acknowledgements

Authors are grateful to TATA Steel Limited, India for funding this research. The authors thank Phenom-World for the use of the Phenom Pro X desktop SEM.

#### Appendix A. Supplementary data

Supplementary data to this article can be found online at <https://doi.org/10.1016/j.wear.2019.03.028>.

#### Funding

This work was supported by TATA Steel Limited, India [Grant number: LJAG895].

#### References

- [1] K. Bhansali, A.E. Miller, Resistance of pure metals to low stress abrasive wear, *Wear* 71 (1981) 375–379.
- [2] K.H.Z. Gahr, *Microstructure and Wear of Materials in Tribology Series* vol. 10, Elsevier, 1987, pp. 1–7.
- [3] Z. Guo, F. Xiao, S. Lu, H. Li, B. Liao, Effects of heat-treatment on the microstructure and wear resistance of a high-chromium cast iron for rolls, *Advances in Materials*

- Science and Engineering (2016) 2016.
- [4] N. Ojala, K. Valtonen, V. Heino, M. Kallio, J. Aaltonen, P. Siitonen, and V. T. Kuokkala, “Effects of Composition and Microstructure on the Abrasive Wear Performance of Quenched Wear Resistant Steels,” vol. vol. 317, pp. 225–232.
- [5] M.M. Khrushchov, Principles of abrasive wear, *Wear* 28 (1974) 69–88.
- [6] L. Qian, X. Xiao, Q. Sun, T. Yu, “Anomalous relationship between hardness and wear properties of a superelastic nickel–titanium alloy, *Appl. Phys. Lett.* 84 (2004) 1076–1078.
- [7] I.M. Hutchings, Wear-resistant materials: into the next century, *Mater. Sci. Eng., A* 184 (1994) 185–195.
- [8] E. Zdravceková, J. Tkáčová, M. Ondáč, et al., Effect of microstructure factors on abrasion resistance of high-strength steels, *Res. Agric. Eng.* 60 (2014) 115–120.
- [9] L. Fang, Q.D. Zhou, Y.J. Li, An explanation of the relation between wear and material hardness in three-body abrasion, *Wear* 151 (1991) 313–321.
- [10] Everhard Abrasion Resistance Steel Plate, JFE Steel corporation, (2019) Available at: <http://www.jfe-steel.co.jp/en/products/plate/b05.html> Accessed 5 Apr. 2019.
- [11] Wear resistance steels, ArcelorMittal, (2019) Available at: <https://industeel.arcelormittal.com/products/wear-resistant-steels/> Accessed 5 Apr. 2019.
- [12] K.H.Z. Gahr, *Microstructure and Wear of Materials. Tribology Series*, Elsevier, Amsterdam ; New York, 1987.
- [13] A. Ball, On the importance of work hardening in the design of wear-resistant materials, *Wear* 91 (1983) 201–207.
- [14] W. Wang, R. Song, S. Peng, Z. Pei, Multiphase steel with improved impact-abrasive wear resistance in comparison with conventional hadfield steel, *Mater. Des.* 105 (2016) 96–105.
- [15] K.H.Z. Gahr, V.D. Doane, Optimizing fracture toughness and abrasion resistance in white cast irons, *Metallurgical Transactions A* 11 (Apr 1980) 613–620.
- [16] M.A. Moore, Abrasive wear, *Int. J. Mater. Eng. Appl.* 1 (1978) 97–111.
- [17] L. Xu, C. Vose, D.S. John, Abrasive wear study of selected white cast irons as liner materials for the mining industry, *Wear* 162 (1993) 820–832.
- [18] S.F. Scieczka, K. Filipowicz, An integrated testing method for cermet abrasion resistance and fracture toughness evaluation, *Wear* 216 (1998) 202–212.
- [19] T. Gladman, D. Dulieu, Grain-size control in steels, *Met. Sci.* 8 (1) (1974) 167–176.
- [20] H.K. Bhadeshia, Strong ferritic-steel welds, 539 *Trans Tech Publ*, 2007, pp. 6–11 *Mater. Sci. Forum.*
- [21] H. Bhadeshia, Bulk nanocrystalline steel, *Ironmak. Steelmak.* 32 (5) (2005) 405–410.
- [22] E. Kozeschnik, H. Bhadeshia, Influence of silicon on cementite precipitation in steels, *Mater. Sci. Technol.* 24 (3) (2008) 343–347.
- [23] V. Ratia, I. Miettunen, V.T. Kuokkala, Surface deformation of steels in impact-abrasion: the effect of sample angle and test duration, *Wear* 301 (2013) 94–101.
- [24] E. Badisch, S. Ilo, R. Polak, Multivariable modeling of impact-abrasion wear rates in metal matrix-carbide composite materials, *Tribol. Lett.* 36 (2009) 55–62.
- [25] V. Ratia, I. Miettunen, V.T. Kuokkala, Surface deformation of steels in impact-abrasion: The effect of sample angle and test duration, *Wear* 301 (2013) 94–101 *Wear of Materials* 2013.
- [26] J. Rendón, M. Olsson, Abrasive wear resistance of some commercial abrasion resistant steels evaluated by laboratory test methods, *Wear* 267 (2009) 2055–2061.
- [27] R.D. Wilson, J.A. Hawk, Impeller wear impact-abrasive wear test, *Wear* 225–229 (Part 2) (1999) 1248–1257.
- [28] A. Sundström, R. José, M. Olsson, Wear behaviour of some low alloyed steels under combined impact/abrasion contact conditions, *Wear* 250 (2001) 744–754.
- [29] J.A. Hawk, R.D. Wilson, J.H. Tylczak, Ö.N. Doğan, Laboratory abrasive wear tests: investigation of test methods and alloy correlation, *Wear* 225–229 (Part 2) (1999) 1031–1042.
- [30] V. Ratia, K. Valtonen, V.T. Kuokkala, “Impact-abrasion wear of wear-resistant steels at perpendicular and tilted angles,” *Proceedings of the Institution of Mechanical Engineers, Participant J.: Journal of Engineering Tribology* 227 (2013) 868–877.
- [31] K. Valtonen, Tampere University of Technology, Publication, Tampere University of Technology, 2018, p. 11.
- [32] S. Chatterjee, H. Bhadeshia, Trip-assisted steels: cracking of high-carbon martensite, *Mater. Sci. Technol.* 22 (2006) 645–649.
- [33] T. Hanamura, S. Torizuka, S. Tamura, S. Enokida, H. i. Takechi, “Effect of austenite grain size on transformation behavior, microstructure and mechanical properties of 0.1 C–5Mn martensitic steel, *ISIJ Int.* 53 (2013) 2218–2225.
- [34] J. Hidalgo, M.J. Santofimia, Effect of prior austenite grain size refinement by thermal cycling on the microstructural features of as-quenched lath martensite, *Metall. Mater. Trans.* 47 (2016) 5288–5301.
- [35] H. Lan, L. Du, Q. Li, C. Qiu, J. Li, R. Misra, Improvement of strength-toughness combination in austempered low carbon bainitic steel: The key role of refining prior austenite grain size, *J. Alloy. Comp.* 710 (2017) 702–710.
- [36] A.-F. Gourgues-Lorenzon, Application of electron backscatter diffraction to the study of phase transformations, *Int. Mater. Rev.* 52 (2007) 65–128.
- [37] A. Sundström, J. Rendón, M. Olsson, Wear behaviour of some low alloyed steels under combined impact/abrasion contact conditions, *Wear* 250 (2001) 744–754 *13th International Conference on Wear of Materials.*
- [38] S.D. Bakshi, *Wear of Fine Pearlite, Nanostructured Bainite and Martensite*, PhD Thesis (2016).
- [39] K. Valtonen, V. Ratia, N. Ojala, V.-T. Kuokkala, Comparison of laboratory wear test results with the in-service performance of cutting edges of loader buckets, *Wear* 388 (2017) 93–100.
- [40] N.P. Suh, An overview of the delamination theory of wear, *Wear* 44 (1977) 1–16.
- [41] B. S. Chahar and A. K. P. Siddhartha, “Erosion Wear of Ductile Materials: A Review,”
- [42] V. Heino, K. Valtonen, P. Kivikytö-Reponen, P. Siitonen, V.-T. Kuokkala, Characterization of the effects of embedded quartz layer on wear rates in abrasive wear, *Wear* 308 (1–2) (2013) 174–179.
- [43] S.D. Bakshi, P.H. Shipway, H.K.D.H. Bhadeshia, Three-body abrasive wear of fine pearlite, nanostructured bainite and martensite, *Wear* 308 (2013) 46–53.